RADIOHELIOGRAPH OBSERVATIONS OF METRIC TYPE II BURSTS AND THE KINEMATICS OF CORONAL MASS EJECTIONS

R. Ramesh[1], C. Kathiravan[1], Sreeja S. Kartha[1], and N. Gopalswamy[2]
[1] Indian Institute of Astrophysics, Bangalore 560 034, India; ramesh@iiap.res.in
[2] NASA Goddard Space Flight Center, Greenbelt, MD, USA

ABSTRACT

Assuming that metric type II radio bursts from the Sun are due to magnetohydrodynamic shocks driven by coronal mass ejections (CMEs), we estimate the average CME acceleration from its source region up to the position of the type II burst. The acceleration values are in the range $\approx$600–1240 m s^{-2}, which are consistent with values obtained using non-radio methods. We also find that (1) CMEs with comparatively larger acceleration in the low corona are associated with soft X-ray flares of higher energy; the typical acceleration of a CME associated with X1.0 class soft X-ray flare being $\approx$1020 m s^{-2}, and (2) CMEs with comparatively higher speed in the low corona slow down quickly at large distances from the Sun—the deceleration of a CME with a typical speed of 1000 km s^{-1} being $\approx$$-15$ m s^{-2} in the distance range of $\approx$3–32 $R_{\odot}$.

Key words: solar–terrestrial relations – Sun: activity – Sun: corona – Sun: radio radiation

1. INTRODUCTION

Solar type II radio bursts are the signatures of magnetohydrodynamic (MHD) shocks propagating outward through the solar atmosphere. They occur frequently as two relatively slow drifting emission bands (fundamental (F) and harmonic (H)) with a frequency ratio of $\approx$1:2. Their drift (typically $\sim$ 0.5 MHz s^{-1}), from high to low frequencies, results from the decrease of plasma density with distance in the solar atmosphere. The characteristics and detailed description of solar type II bursts can be found in Nelson & Melrose (1985), Mann et al. (1995), Aurass (1997), and Gopalswamy (2006). Coronal mass ejections (CMEs), flares, expanding soft X-ray features, coronal waves, small-scale ejecta like sprays, soft X-ray jets, and plasmoids, erupting loops have all been proposed as likely candidates for the driver of MHD shocks leading to metric type II bursts (Nindos et al. 2008; Pick & Vilmer 2008 and the references therein). However, statistical results using white light, X-ray, Hα, and radio spectral observations indicate that most of the metric type II bursts can be explained by CME-driven shocks (Claßen & Aurass 2002; Cliver et al. 2004; Mancuso & Raymond 2004; Cho et al. 2005, 2008; Gopalswamy 2006). The metric type II bursts typically occur in the radial distance range $\approx$1–2 $R_{\odot}$. It is difficult to observe CMEs and estimate their speed/acceleration in this distance range due to observational constraints. Since metric type II bursts are considered to be one of the earliest signatures of shocks in the solar corona, we were interested in investigating the kinematics of the CMEs in the above distance range particularly with radioheliograph data since the assumptions are less here. Hence the present work.

2. THE DATA SET

The type II bursts used in the present study were obtained at 109 MHz during 1997–2005 with the Gauribidanur radioheliograph (GRH; Ramesh et al. 1998) located about 100 km north of Bangalore in India.[3] The GRH is a T-shaped radio interferometer array dedicated for observations of the solar corona in the frequency range 40–120 MHz and time interval $\approx$4–9 UT. It was

commissioned in 1997 and is in regular operation since then. The angular resolution of the array at its zenith is $\approx$7$'$ × 10$'$ (R.A. × decl.) at 109 MHz. The minimum detectable flux at 109 MHz is $\approx$200 Jy. The coordinates of the array are Longitude = 77°27$'$07$''$ East and Latitude = 13°36$'$12$''$ North. Though a large number of type II bursts were observed with the GRH during the above period, we specifically selected only those events whose Hα flares were located at heliographic longitude $\geqslant$ 45° and projected radial distance (r) $\geqslant$ 0.7 $R_{\odot}$ for the present work. This minimizes possible projection effects. Due to radio interference and the need for higher angular resolution, observations with the GRH were limited to a single frequency (109 MHz) during most of the time. With these limitations, we could get seven events during the period 1997–2005. We used data obtained with the Large Angle and Spectrometric Coronagraph (LASCO; Brueckner et al. 1995) onboard *Solar and Heliospheric Observatory* (*SOHO*) for information on the associated white light CMEs. The solar sources of the CMEs were identified as the location of the associated Hα flares listed in Solar Geophysical Data (SGD).[4] The same was also verified from the brightening observed in the EUV images obtained with Extreme-ultraviolet Imaging Telescope (EIT; Delaboudiniere et al. 1995) onboard *SOHO*.

Figure 1 shows a composite of the GRH radioheliogram obtained at 05:08 UT and the LASCO + EIT 195 Å difference image observed 05:30 UT and 05:24 UT, respectively, on 2005 August 3. According to SGD, a type II burst with both F and H components was observed during 05:03–05:12 UT on 2005 August 3. The respective components were observed over the frequency range $\approx$85–35 MHz and 160–50 MHz during the above period. This indicates that the discrete source of intense radio emission contours in Figure 1 must be the harmonic component. The projected radial distance and position angle (PA; measured counterclockwise from the solar north) of the burst at 109 MHz are $\approx$1.3 $R_{\odot}$ and 106°, respectively. The radio event was associated with a M3.4 class soft X-ray flare observed by the X-ray sensor onboard *Geostationary Operational Environmental Satellite* (*GOES*) from the heliographic location S13 E45 (inferred from the corresponding Hα flare coordinates

---

[3] http://www.iiap.res.in/centers/radio

[4] http://sgd.ngdc.noaa.gov/sgd/solarindex.jsp

Table 1
Details of the Metric Type II Bursts and the Associated Hα/X-ray Flares

Date	Type II Burst			Flare Details			
	Time t_{typeII} (UT)	Proj. r_{typeII} ($R_\odot$)	PA (deg)	Onset–Peak Time (UT)	X-ray Imp.	Hα Posn.	Proj. $r_{\mathrm{H\alpha}}$ ($R_\odot$)
(1)	(2)	(3)	(4)	(5)	(6)	(7)	(8)
1999 Mar 8	06:40	1.20	98	06:30–06:37	M2.6	S24E93	0.99
2000 Sep 9	08:41	1.10	298	08:28–08:49	M1.6	N07W53	0.80
2004 Jan 7	04:01	1.50	114	03:43–04:40	M4.5	N02E82	0.99
2005 Jan 19	08:16	1.30	300	08:03–08:22	X1.3	N19W47	0.76
2005 Jul 27	04:47	1.40	100	04:33–05:02	M3.7	N11E90	1.00
2005 Jul 30	06:32	1.50	71	06:17–06:35	X1.3	N12E60	0.87
2005 Aug 3	05:08	1.30	106	04:54–05:06	M3.4	S13E45	0.73

given in SGD). The X-ray flare started at 04:54 UT and its peak was at 05:06 UT. An inspection of the LASCO CME catalog (Gopalswamy et al. 2009a)[5] revealed that a CME at PA ≈104° and width ≈65° was observed in close association with the type II burst and flare. The extrapolated onset time of the CME at $r = 1$ $R_\odot$ was 04:55 UT. The first height–time measurement of the CME (CME-ht1) was at $t_{\mathrm{CMEht1}} \approx 05:30$ UT when its leading edge (LE) was located at $r_{\mathrm{CMEht1}} \approx 2.71$ $R_\odot$ in the LASCO field of view (FOV) from ≈3 to 32 $R_\odot$. Its average speed in the latter (i.e., v_{LASCO}) was ≈479 km s^{-1}. The average acceleration of the CME between its first and last observed locations (2.71 and 19.81 $R_\odot$) in the LASCO FOV (i.e., a_{LASCO}) was ≈−6.7 m s^{-2}. Similar information for all the other radio and flare events considered for the present study are provided in Table 1. The date and time of occurrence (hh:mm format) of type II burst at 109 MHz are listed in Columns 1 and 2. Their projected radial distance (i.e., r_{typeII}) and position angle are given in Columns 3 and 4. The error in the estimated type II burst location is ≈±0.2 $R_\odot$ and is primarily due to the coarse angular resolution of the GRH. The onset and peak time of the associated *GOES* soft X-ray flares and their class are given in Columns 5 and 6. The heliographic coordinates of the corresponding Hα flares and their projected radial distance are given in Columns 7 and 8. Information on the CMEs obtained from the *SOHO*/LASCO CME catalog are listed in Columns 2–8 of Table 2. The CME parameters derived from the GRH observations are provided in Table 3.

The shift in the solar radio source position due to ionospheric effects was found to be ≲ 0.1 $R_\odot$ at 80 MHz in the hour angle range ±2 hr (Stewart & McLean 1982). At 109 MHz, the error is expected to be smaller. Similarly, effects of scattering ("irregular refraction") on the observed source position/height are also considered to be very small at 109 MHz compared to lower frequencies (Aubier et al. 1971). Ray-tracing calculations employing more realistic coronal electron density models and density fluctuations show that the turning points of the rays that undergo irregular refraction due to density inhomogeneities in the solar corona almost coincide with the location of the plasma ("critical") layer in the non-scattering case even at 73.8 MHz (Thejappa & MacDowall 2008). Obviously, the situation should be still better at 109 MHz. Moreover, observations of source sizes smaller than predicted by the scattering theory have been reported by Kerdraon (1979) at 169 MHz, Ramesh et al. (1999) at 75 MHz, and Ramesh & Sastry (2000) at 34.5 MHz. An inspection of SGD indicates that all the type II bursts at 109 MHz

---
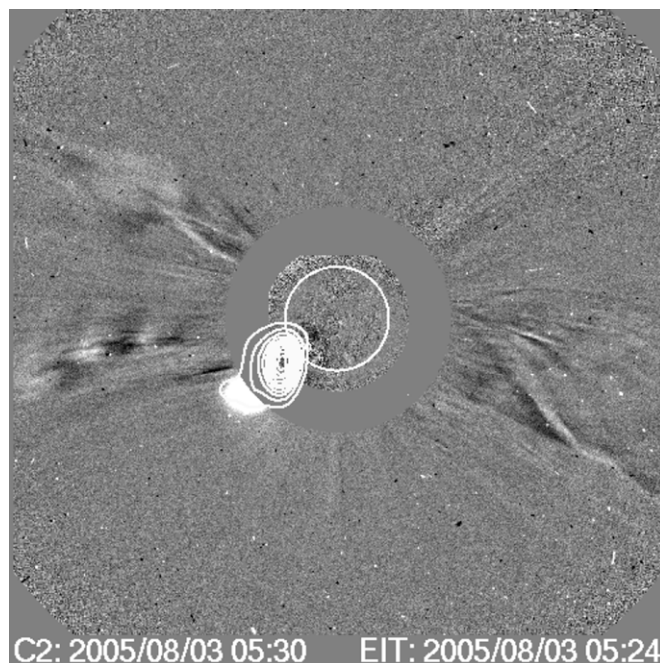
Figure 1. Composite of the radioheliogram of the type II burst of 2005 August 3 observed with the GRH at 109 MHz and the associated LASCO C2 + EIT 195 Å difference image. Solar north is straight up and east is to the left. The inner white circle at the center represents the solar limb. The outermost gray circle indicates the occulting disk of the LASCO C2 coronagraph. Its radius is ≈2.2 $R_\odot$. The bright white light emission above the southeast quadrant of the coronagraph occulter is the CME under study. The dimming close to the southeast limb in the EIT image is the flare location. The intense discrete radio source located between the aforementioned white light structure and the solar limb is the type II burst under study. It was observed at $r = 1.3$ $R_\odot$ around 05:08 UT, about 22 minutes before the first appearance of the white light CME at $r = 2.71$ $R_\odot$ in the LASCO FOV (see Tables 1 and 2 for details). The peak brightness temperature (T_b) of the radio source is ≈4 × 10^8 K. The contours are in interval of 10% of the peak T_b and the outermost contour corresponds to $T_b \approx 1.2 \times 10^8$K.

Table 2
Details of the CMEs Associated with the Metric Type II Bursts in Table 1

Date	Measurements from *SOHO*/LASCO CME Catalog						
	Onset Time at 1 $R_\odot$ (UT)[a]	Crossing Time of Type II Location (UT)[a]	First Obs. t_{CMEht1} (UT)	CPA/ Width (deg)[b]	Lead. Edge r_{CMEht1} ($R_\odot$)[a,b]	Speed (km s^{-1})[c] v_{LASCO}	Accln. (m s^{-2})[a] a_{LASCO}
(1)	(2)	(3)	(4)	(5)	(6)	(7)	(8)
1999 Mar 8	06:33	06:36	06:54	115/80	2.30	664	−10
2000 Sep 9	08:21	08:23	08:56	271/180	3.22	554	−13.4
2004 Jan 7	03:54	03:57	04:06	78/171	3.00	1581	−60.4
2005 Jan 19	08:11	08:13	08:29	321/70	4.54	2020	−43.8
2005 Jul 27	04:43	04:45	04:54	84/75	2.92	1787	−75.4
2005 Jul 30	06:27	06:30	06:50	50/106	5.65	1968	−102.6
2005 Aug 3	04:55	05:01	05:30	104/65	2.71	479	−6.7

Notes.
[a] Based on quadratic fit to the height–time measurements.
[b] At the first appearance in the *SOHO*/LASCO C2 FOV.
[c] Based on linear fit to the height–time measurements.

considered for the present study are harmonic components. This is expected since the fundamental component in the case of limb type II bursts may be occulted by the overlying corona and hence do not reach the observer (Nelson & Melrose 1985).

Table 3
CME Parameters Derived from the GRH Observations

Date	Computed LE from Type II Data $(R_\odot)$[a]	Speed v_{typeII} at Type II Onset (km s^{-1})	Accln. a_{typeII} at Type II Onset (m s^{-2})	Speed v_{CMEht1} at First Appearance in LASCO C2 (km s^{-1})[b]
(1)	(2)	(3)	(4)	(5)
1999 Mar 8	2.2	487	812	911
2000 Sep 9	2.2	535	686	1640
2004 Jan 7	1.8	657	609	3480
2005 Jan 19	2.9	964	1236	2891
2005 Jul 27	1.9	663	789	2519
2005 Jul 30	3.9	974	1083	2674
2005 Aug 3	4.5	945	1124	743

Notes.
[a] At the first appearance in the *SOHO*/LASCO C2 FOV.
[b] Based on linear fit to the type II and first appearance in *SOHO*/LASCO C2 FOV height–time measurements.

3. ANALYSIS AND RESULTS

It has been suggested that the type II bursts occur following the peak of the associated flare in the flare–type II scenario (Claßen & Aurass 2002; Shanmugaraju et al. 2003a). However, we find from SGD that the start time of all the type II bursts in Table 1 at their highest observed frequency (>109 MHz) was before the peak of the associated flare, i.e., they were during the onset-peak phase of the flare. We see from Columns 2 and 5 of Table 1 that this is true even at 109 MHz—most of the type II bursts occurred before the flare peak. Since the radial distance of all the flares (i.e., $r_{H\alpha}$) listed in Table 1 are close to the limb (Column 8 in Table 1), the onset times of the associated CMEs must be without much projection effect. We find that the bursts had occurred after the extrapolated onset time of the associated CME at $r = 1$ $R_\odot$ (Column 2 in Tables 1 and 2). Also the CMEs were at the radial distance corresponding to the type II bursts at 109 MHz well before the peak of the associated X-ray flares (Column 5 in Table 1 and Column 3 in Table 2).

These temporal relationships are consistent with the current paradigm of flare–CME connection and that the type II bursts are due to CME-driven shocks. Moreover, recent observations with the inner coronagraph (COR1) of the Sun–Earth Connection Coronal and Heliospheric Investigation (SECCHI; Howard et al. 2008) instrument onboard *Solar TErrestrial RElations Observatory* (*STEREO*; Kaiser et al. 2008) indicate that MHD fast-mode shocks form very low in the corona, when the CME LE is only at a distance of $r \sim 1.5$ $R_\odot$ (Gopalswamy et al. 2009b). Earlier, Zhang et al. (2001) had pointed out that CMEs are initiated at a height of 1.3–1.5 $R_\odot$. The radial distance (r_{typeII}) of the type II bursts listed in Column 3 of Table 1 are consistent with the above results within the error limits. It has also been reported that (1) the acceleration of the CMEs is closely synchronized with the growth of the associated soft X-ray flare (Zhang et al. 2001; Alexander et al. 2002; Gallagher et al. 2003; Shanmugaraju et al. 2003b) and continues after the flare maximum (Maričić et al. 2007) and (2) type II bursts observed in association with the CMEs are due to shock driven by the latter during their passage through the low corona, we assume that the source region of the CMEs to be the same as the location of the corresponding Hα flares and the type II bursts reported were due to MHD shocks driven by the CMEs during their passage through the low corona, we

estimated the acceleration of the CMEs at type II onset (i.e., a_{typeII} at t_{typeII}) using the kinematic equation, $s = ut + 0.5at^2$. Here, s is the separation between the location of the Hα flare and type II burst at 109 MHz, and t is the time interval between the onset of the flare and the occurrence of the type II burst at 109 MHz. We further assumed that (1) the initial CME velocity $u = 0$, since the CME is considered to start from rest as it erupts (Gopalswamy et al. 2009b) and (2) the type II bursts are located close to the LE of the associated CMEs (Maia et al. 2000). The latter assumption holds good for all the bursts in our list except for the event of 2005 January 19 which is located approximately midway between the LE and flank of its associated CME (Column 4 in Table 1 and Column 5 in Table 2). Considering the event of 2005 August 3 shown in Figure 1, we find that the flare started around 04:54 UT from the heliographic location S13E45. The latter corresponds to $r_{H\alpha} \approx 0.73$ $R_\odot$. The associated type II burst observed with the GRH at 109 MHz around 05:08 UT was located at $r_{typeII} \approx 1.3$ $R_\odot$. From the above two values of r, we get $s = r_{typeII} - r_{H\alpha} = 0.57$ $R_\odot$ for this event. The corresponding time difference is $t = t_{typeII} - t_{H\alpha} = 840$s. Substituting these values in the aforementioned kinematic equation, we get $a_{typeII} \approx 1124$ m s^{-2}. Similarly, we also calculated the velocity of the above CME at type II onset (i.e., v_{typeII} at t_{typeII}) using the kinematic equation, $v = u + at$. The terms a, u, and t are the same as defined above. Assuming $u = 0$ as earlier and substituting for a and t, we find that $v_{typeII} \approx 945$ km s^{-1}. We then computed the location of LE of the CME (at the first appearance in the LASCO C2 FOV) using the above values of v_{typeII} and a_{typeII} in the kinematic equation, $s = ut + 0.5at^2$. Here, s is the distance traveled by the CME in the time interval t between type II onset t_{typeII} and the first appearance time t_{CMEht1} in the LASCO C2 FOV (as per the catalog), $a = a_{typeII}$ and $u = v_{typeII}$. We find that the CME should be at a radial distance of ≈ 4.5 $R_\odot$. The above as well as similar results for the other events are listed in Columns 2, 3, and 4 of Table 3. We find that a_{typeII} for the events in our list is in the range $\approx 610–1240$ m s^{-2}. These values are consistent with the CME acceleration in the low corona reported by St. Cyr et al. (1999), Wood et al. (1999), Zhang et al. (2001), and Vršnak et al. (2007) using non-radio data.

The CME acceleration in the low corona is significantly different from the deceleration derived using the LASCO data. This is because LASCO does not "see" the acceleration phase of the CMEs due to FOV restrictions. In fact, if we use the positive acceleration (a_{typeII}) determined above, the CME speed (v_{typeII}) at the time of type II onset (t_{typeII}) is well below the *SOHO*/LASCO CME catalog speed (v_{LASCO}), demonstrating that the CMEs are still accelerating at the time of type II burst onset (Column 7 of Table 2 and Column 3 of Table 3). The single exception was the event of 2005 August 3, which finished accelerating well before the onset of the type II burst. Two such impulsive events were reported in Gopalswamy et al. (2009b). If we use the *SOHO*/LASCO catalog acceleration (a_{LASCO}), we see that the type II bursts generally occur after CMEs have crossed the type II location, which might lead to the conclusion that the type II burst location (r_{typeII}) is behind the CME LE at type II onset t_{typeII} (Column 2 in Table 1 and Column 3 in Table 2). However, when we compute the latter using the a_{typeII} mentioned above, the type II burst location is at or above the LE at t_{typeII}. For example, the computed CME LE at t_{CMEht1} using a_{typeII} is well below the observed CME LE r_{CMEht1} at t_{CMEht1} (Column 6 in Table 2 and Column 2 in Table 3), except for the 2005 July 30 event (see below). For the same reason,
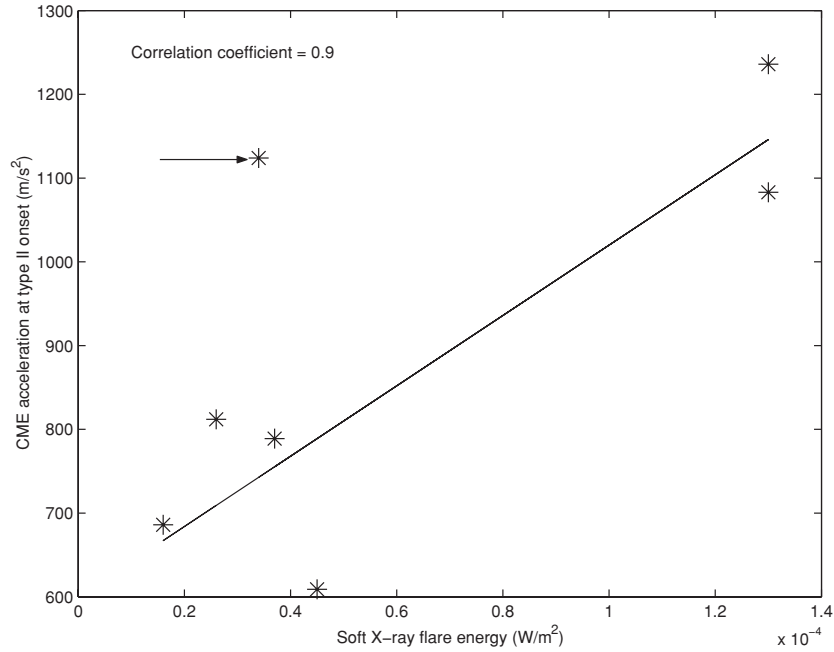
Figure 2. Variation of the estimated average CME acceleration a_{typeII} in the low corona with the *GOES* soft X-ray flare energy. From the parameters of linear fit ($y = 4.2 \times 10^6 x + 600$) to the data points, we find that the typical acceleration of a CME associated with X1.0 class flare (energy $= 10^{-4}$ W m^{-2}) will be $\approx$1020 m s^{-2}. The point indicated by the arrow mark corresponds to the event of 2005 August 3 for which the CME speed v_{typeII} in the low corona is higher compared to the LASCO speed v_{LASCO} (see the corresponding entries in Column 7 of Table 2 and Column 3 of Table 3).

the 1 $R_\odot$ onset times of the CMEs listed in Table 2 are also not accurate when we use the LASCO decelerations, which give later liftoff time for the CMEs. In other words, the type II burst is always formed after the liftoff time of the CMEs. In some events, type II bursts started at frequencies higher than 109 MHz, as reported in SGD. Even in these cases, the onset time of type II bursts was after the 1 $R_\odot$ liftoff time. The only exception was the 2005 July 30 event in which the type II onset preceded the CME liftoff by $\sim$ 6 minutes. The first appearance of the CME was at a heliocentric distance of 5.6 $R_\odot$, which requires too much extrapolation. Furthermore, inclusion of the acceleration phase would yield a much earlier liftoff time for the CME.

Various studies indicate that the CME dynamics is closely related to the energy release in the associated flare (Moon et al. 2002; Burkepile et al. 2004). Since metric type II bursts are one of the earliest signature of shocks in the solar corona and can be observed closer to the Sun than the white light CMEs, we compared the CME acceleration (a_{typeII}) values at type II onset t_{typeII} with the flux of the associated *GOES* X-ray flare. Figure 2 shows the results of our work. There is a positive correlation ($\approx$0.9) between the flare energy and the CME acceleration, i.e., CMEs associated with flares of larger energy exhibit higher acceleration. We find that the typical acceleration of a CME associated with X1.0 class flare (energy $= 10^{-4}$ W m^{-2}) is $\approx$1020 m s^{-2}. A similar result was reported recently by Maričić et al. (2007) using white light and non-radio observations of CME signatures. The authors obtained a correlation of $\approx$0.6 for their sample of the events.

Next, we compared the speed of the CMEs (v_{typeII}) close to type II onset (t_{typeII}) and in the LASCO FOV (v_{LASCO}). The latter was taken from the catalog (Column 7 of Table 2) and was found to be greater than v_{typeII}. This is consistent with the recent results of Gopalswamy et al. (2009b): there is an increase in the CME speed between the inner and outer corona

as revealed by SECCHI/COR1 and LASCO, for a majority of the CMEs. We also find from the above calculations that the lowest speed of the CME in the low corona is $\approx$487 km s^{-1} (Column 3 in Table 3). According to Gopalswamy et al. (2001a), disturbances exceeding a speed of $\sim$230 km s^{-1} in the distance range $r \leqslant 1.4$ $R_\odot$ may be super-Alfvénic and produce fast-mode shocks in the quiet corona surrounding active regions. This again reinforces our initial assumption that the type II bursts reported are likely due to MHD shocks driven by the CMEs.

Finally, we find that all the seven CMEs exhibit deceleration in the LASCO FOV. We used the speed of the CMEs at their first appearance in the LASCO C2 FOV (i.e., $v_{CMEht1} = [r_{CMEht1} - r_{typeII}]/[t_{CMEht1} - t_{typeII}]$) for this purpose. The individual values of r and t used in the above calculation are listed in Columns 2 and 3 of Table 1 and Columns 4 and 6 of Table 2. The CMEs with large speed in the low corona slow down much faster in the LASCO FOV than did the slower CMEs (Column 5 in Table 3 and Column 8 in Table 2). The deceleration in the LASCO FOV is $\approx$−15 m s^{-2} for CMEs with speed 1000 km s^{-1} in the low corona (Figure 3). This result is similar to that obtained by Gopalswamy et al. (2001b) for the CMEs associated with type II radio bursts at decameter–hectometer (DH) wavelengths. The authors found that acceleration is anticorrelated (correlation coefficient $\approx$0.76) with the speed, i.e., the faster CMEs decelerate more than the slower CMEs. This is close to the value of $\approx$−0.79 obtained in the present case (Figure 3). We also found the correlation coefficient for the present set of events using the CME speeds in the LASCO FOV (Column 7 of Table 2) and value is $\approx$−0.86 (Figure 3), almost same as our above estimate of $\approx$0.79 using type II bursts. In a later paper, Gopalswamy et al. (2005) had pointed out that the larger deceleration of faster CMEs is expected because of the aerodynamic drag faced by the CMEs as they propagate into the corona and the interplanetary (IP) medium.
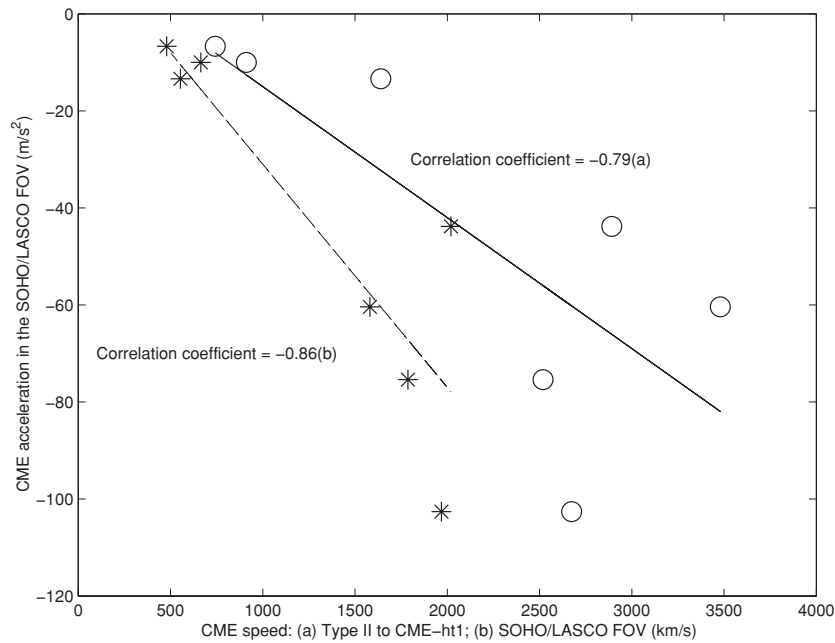
Figure 3. Variation of the CME acceleration a_{LASCO} in the *SOHO*/LASCO FOV ($\approx$3–30 $R_\odot$) with the estimated speed of the CME. The symbol "o" represents the CME speed v_{CMEht1} between type II position and CME-ht1 (a), and "*" corresponds to the CME speed v_{LASCO} from the *SOHO*/LASCO height–time measurements (b). The linear fit $y = -0.027x + 12$ to (a) indicates that a CME with speed of 1000 km s^{-1} in the low corona decelerates typically at the rate of ≈-15 m s^{-2} in the outer corona.

4. CONCLUSIONS

We studied seven near-limb metric type II radio bursts observed with the GRH at 109 MHz during the period 1997–2005. Without assuming any coronal density model and Sunward extrapolation of the height–time measurements of the white light CMEs observed at larger distances from the Sun, we obtained the following results. (1) The acceleration of the CMEs in the low corona and the flux of the associated *GOES* soft X-ray flares are correlated, i.e., CMEs with comparatively larger acceleration are associated with more energetic flares. (2) The speed of the CMEs in the low corona and their acceleration in the outer corona are anticorrelated, i.e., CMEs with larger speed close to the Sun decelerate strongly at large distances from the Sun. But, (1) our sample size is relatively small, and (2) we have assumed that the type II bursts reported are located radially above the associated flare and driven by the LE of the associated CMEs for our calculations. It is possible that the type II burst location in both the above cases are non-radial as revealed by some of the earlier observations (see Klein et al. 1999 and references therein). This would mean that the CME speed and acceleration in the low corona that we have estimated would be the lower limits. (3) The present angular resolution of the GRH is not sufficient to exactly locate the type II bursts in the low corona and our estimate of CME speed and acceleration in the low corona depend critically on the burst location. Nevertheless, the consistency of our results with those reported earlier using non-radio observations clearly indicate that similar radioheliograph studies in the future with higher angular resolution and particularly overlapping with SECCHI/COR1 data in the spatial as well as the temporal domains, might be useful to improve our understanding on the evolution of the CMEs in the low corona. Work is in progress to improve the angular resolution as well as the sensitivity of the GRH by about 2 orders of magnitude.

REFERENCES

Alexander, D., Metcalf, T. R., & Nitta, N. V. 2002, Geophys. Res. Lett., 29, 41
Aubier, M., Leblanc, Y., & Boischot, A. 1971, A&A, 12, 435
Aurass, H. 1997, in Coronal Physics from Radio and Space Observations, Lecture Notes in Physics, ed. G. Trottet (Berlin: Springer), 135
Brueckner, G. E., et al. 1995, Sol. Phys., 162, 357
Burkepile, J. T., et al. 2004, J. Geophys. Res., 109, A03103
Cho, K.-S., et al. 2005, J. Geophys. Res., 110, A12101
Cho, K.-S., et al. 2008, A&A, 491, 873
Claßen, H. T., & Aurass, H. 2002, A&A, 384, 1098
Cliver, E. W., Nitta, N. V., Thompson, B. J., & Zhang, J. 2004, Sol. Phys., 225, 105
Delaboudiniere, J.-P., et al. 1995, Sol. Phys., 162, 291
Gallagher, P. T., Lawrence, G. R., & Dennis, B. R. 2003, ApJ, 588, L53
Gopalswamy, N. 2006, in Geophys. Monogr. Ser. 165, Solar Eruptions and Energetic Particles, ed. N. Gopalswamy, R. Mewaldt, & J. Torsti (Washington, DC: AGU), 207
Gopalswamy, N., et al. 2001a, J. Geophys. Res., 106, 25261
Gopalswamy, N., et al. 2001b, J. Geophys. Res., 106, 29219
Gopalswamy, N., et al. 2005, J. Geophys. Res., 110, A12S07
Gopalswamy, N., et al. 2009a, Earth Moon Planets, 104, 295
Gopalswamy, N., et al. 2009b, Sol. Phys., 259, 227
Howard, R. A., et al. 2008, Space Sci. Rev., 136, 67
Kaiser, M. L., et al. 2008, Space Sci. Rev., 136, 5
Kerdraon, A. 1979, A&A, 71, 266
Klein, K.-L., et al. 1999, A&A, 346, L53
Maia, D., Pick, M., Vourlidas, A., & Howard, R. 2000, ApJ, 528, L49
Mancuso, S., & Raymond, J. C. 2004, A&A, 413, 363
Mann, G., Classen, T., & Aurass, H. 1995, A&A, 295, 775
Maričić, D., et al. 2007, Sol. Phys., 241, 99
Moon, Y.-J., et al. 2002, ApJ, 581, 694

Nelson, G. J., & Melrose, D. B. 1985, Solar Radiophysics (Cambridge: Cambridge Univ. Press), 333

Neupert, W. M., Thompson, B. J., Gurman, J. B., & Plunkett, S. P. 2001, J. Geophys. Res., 106, 25215

Nindos, A., Aurass, H., Klein, K.-L., & Trottet, G. 2008, Sol. Phys., 253, 3

Pick, M., & Vilmer, N. 2008, A&AR, 16, 1

Ramesh, R., & Sastry, Ch. V. 2000, A&A, 358, 749

Ramesh, R., Subramanian, K. R., & Sastry, Ch. V. 1999, Sol. Phys., 185, 77

Ramesh, R., Subramanian, K. R., Sundararajan, M. S., & Sastry, Ch. V. 1998, Sol. Phys., 181, 439

Shanmugaraju, A., Moon, Y.-J., Dryer, M., & Umapathy, S. 2003a, Sol. Phys., 215, 161

Shanmugaraju, A., Moon, Y.-J., Dryer, M., & Umapathy, S. 2003b, Sol. Phys., 215, 185

St. Cyr, O. C., Burkepile, J. T., Hundhausen, A. J., & Lecinski, A. R. 1999, J. Geophys. Res., 104, 12493

Stewart, R. T., & McLean, D. J. 1982, PASA, 4, 386

Thejappa, G., & MacDowall, R. J. 2008, ApJ, 676, 1338

Vršnak, B., et al. 2007, Sol. Phys., 241, 85

Wood, B. E., et al. 1999, ApJ, 512, 484

Zhang, J., et al. 2001, ApJ, 559, 452